Chemical Science

EDGE ARTICLE

View Article Online
View Journal | View Issue

Cite this: *Chem. Sci.*, 2019, **10**, 10106

All publication charges for this article have been paid for by the Royal Society of Chemistry

Development of a novel anti-tumor theranostic platform: a near-infrared molecular upconversion sensitizer for deep-seated cancer photodynamic therapy†

Ruisong Tian,[a] Wen Sun,[ab] Mingle Li,[a] Saran Long,[ab] Miao Li,[a] Jiangli Fan,[ab] Lianying Guo[c] and Xiaojun Peng *[ab]

Received 13th August 2019
Accepted 11th September 2019

DOI: 10.1039/c9sc04034j

rsc.li/chemical-science

Upconversion-based photon-initiated therapeutic modalities, photodynamic therapy (PDT) in particular, have shown significant clinical potential in deep-seated tumor treatment. However, traditional multiphoton upconversion materials involving lanthanide (ion)-doped upconversion nanoparticles (UCNPs) and two-photon absorption (TPA) dyes often suffer from lots of inherent problems such as unknown systematic toxicity, low reproducibility, and extremely high irradiation intensity for realization of multiphoton upconversion excitation. Herein, for the first time, we report a one-photon excitation molecular photosensitizer (FUCP-1) based on a frequency upconversion luminescence (FUCL) mechanism. Under anti-Stokes (808 nm) excitation, FUCP-1 showed excellent photostability and outstanding upconversion luminescence quantum yield (up to 12.6%) for imaging-guided PDT. *In vitro* cellular toxicity evaluation presented outstanding inhibition of 4T1 cells by FUCP-1 with 808 nm laser irradiation (the half maximal inhibitory concentration was as low as 2.06 μM). After intravenous injection, FUCP-1 could specifically accumulate at tumor sites and obviously suppress the growth of deep-seated tumors during PDT. More importantly, FUCP-1 could be fully metabolized from the body within 24 h, thus dramatically minimizing systemic toxicity. This study might pave a new way for upconversion-based deep-seated cancer PDT.

Introduction

Photodynamic therapy (PDT), a clinically approved noninvasive cancer treatment modality, has attracted considerable attention in recent years.[1–4] PDT agents, also known as photosensitizers (PSs), are generally nontoxic to nonirradiated normal cells and become highly toxic in tumor cells under selective irradiation of the tumor region through generating singlet oxygen ($^1O_2$) or reactive free radicals.[5] Most conventional PSs (*e.g.*, ZnPc, PPIX, *etc.*) are responsive to visible light (400–700 nm); thus, PDT is typically triggered by using visible light.[6,7] However, the tissue penetration limitation of short-wavelength light caused by strong absorption of melanin and hemoglobin in the visible region is problematic for the widespread clinical use of PDT.[7–11] In contrast, near-infrared (NIR) light in the "therapeutic window" (700–900 nm) can effectively penetrate into deeper tissue and causes less photodamage.[12–14] Therefore, it is desirable to realize deep PDT using NIR light, which is of great importance for further clinical applications.

Current efforts have been focused on the red-shift of organic PSs to the NIR region for deep-tissue PDT. However, these compounds are always difficult to synthesize and display bad anti-bleaching capabilities during NIR light irradiation.[7,15,16] Furthermore, as the photon energy of NIR light rapidly decreases above 800 nm, few NIR organic molecules hold promise for effectively generating cytotoxic reactive oxygen species (ROS) and killing tumor cells, especially the deep-seated ones.[17,18]

To overcome these "Achilles' heels", upconversion strategies which can convert low-energy long-wavelength photons to high-energy short-wavelength emission light have become the focus of deep-seated cancer PDT recently.[7] In particular, lanthanide-based multiphoton upconversion nanoparticles (UCPNs) that give rise to ultraviolet-visible light when the lanthanide ions in excited states absorb energies from two or more NIR photons (Scheme 1, left) and then sensitize PSs through a fluorescence resonance energy transfer (FRET) process to generate cytotoxic ROS have presented great potential in deep-seated tumor PDT.[19] Moreover, compared to conventional PSs, UCPNs show

[a]State Key Laboratory of Fine Chemicals, Dalian University of Technology, Dalian 116024, China. E-mail: pengxj@dlut.edu.cn

[b]Research Institute of Dalian University of Technology in Shenzhen, Shenzhen 518057, China

[c]Department of Pathophysiology, Dalian Medical University, Dalian 116044, China

† Electronic supplementary information (ESI) available. See DOI: 10.1039/c9sc04034j

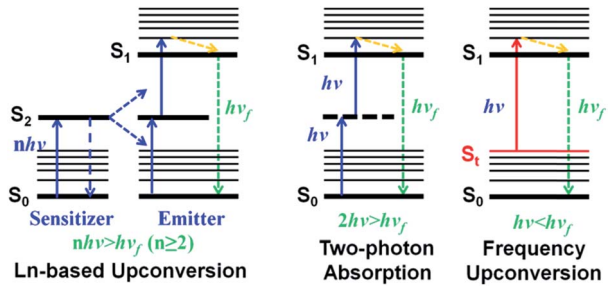

Scheme 1 Schematic illustration of lanthanide-based upconversion (left), two-photon absorption (middle) and frequency upconversion luminescence (right).

a superior *in vivo* tumor imaging effect due to their specific optical properties, such as better tissue penetration depth, large anti-Stokes shift, high signal-to-noise ratio (SNR), and negligible autofluorescence from biological organization.[5,20–22] However, the well-known low reproducibility, potential long-term toxicity and unclear systematic clearance of these upconversion nano-materials may limit their further clinical application.[23–26] Besides, current clinical and experimental data show that the enormous diameters of nano-materials make it difficult for them to penetrate into tumor tissues from blood, leading to a poor PDT effect.[27–32] In addition, non-degradable inorganic nanoparticles through intravenous injection into animal models can unexpectedly promote the intravasation and extravasation of cancer cells.[33] In comparison, organic small molecular PSs feature outstanding merits such as superior biosafety, precise synthesis, and optimal reproducibility, and thus, developing organic molecular upconversion PSs may be of more clinical benefit for cancer therapy.

Alternatively, two-photon absorption (TPA) molecular dyes are another commonly used candidate for deep PDT based on the upconversion mechanism. During the TPA process, a virtual level occurs because of the interaction of photons and dye molecules (Scheme 1, middle).[19] However, the probability of TPA occurring is very low as the virtual level does not really exist. And thus, the realization of two-photon excitation always needs extremely high energy from a femtosecond laser, which can irreversibly damage cells and tissues. Besides, two-photon excitation only occurs at the focus of the high-intensity laser, which makes deep-tissue PDT impractical, because a laser beam will defocus while passing through tissue.[34] These limitations seriously hinder the *in vivo* application of TPA PSs. Therefore, the exploitation of new molecular PSs with a more biocompatible upconversion strategy is greatly desired.

As a potential alternative, frequency upconversion luminescence (FUCL) which is a typical one-photon process, offers a new opportunity for the realization of deep PDT. This FUCL phenomenon was first discovered by Wood in 1928.[27] Early investigations of the FUCL technology were mainly concentrated on the study of the photophysical process, laser cooling and thermal imaging. Quite recently, Li *et al.* used FUCL compounds for the detection of $MeHg^{+}$ and Cu^{2+}, further expanding the application of the FUCL technology.[35,36]

Compared to the multiphoton upconversion mechanism including lanthanide-based f–f transition and TPA, FUCL can be realized when a molecule in the thermally vibrational–rotational state (S_t) absorbs less energy ($h\nu < h\nu_f < nh\nu$, $n \geq 2$) from only one photon (Scheme 1, right).[7,24,37] Moreover, the thermally vibrational–rotational state (S_t) is a real intermediate state, and thus the probability of occurrence of hot band absorption and reaching the excited state (S_1) has a much higher degree than that of TPA. Therefore, these types of organic molecules may be more promising for biological applications, especially deep-seated tumor treatment. Unfortunately, to date, no research based on the FUCL technology has been developed and reported for anti-tumor therapy.

Here, for the first time, we designed and synthesized a one-photon excitation organic molecular upconversion sensitizer (FUCP-1) based on the FUCL mechanism for deep-seated tumor PDT. A rhodamine derivate is chosen because its rhodamine architecture possesses superior capability of hot-band absorption for generating anti-Stokes emission. In FUCP-1, as illustrated in Fig. 1, the introduction of a heavy atom (iodine atom) significantly facilitates the transition of the excited singlet state S_1 to the excited triplet state (T_1), also known as intersystem crossing (ISC) during the one-photon upconversion PDT process. The enhanced ISC ability subsequently promoted the production of cytotoxic singlet oxygen ($^1O_2$).[38–42] Different from conventional Stokes excitation, the one-photon driven upconversion process of FUCP-1 is induced by 808 nm excitation from the thermally excited vibrational–rotational energy sublevels of the ground electronic state S_t to S_1 and the additional energy is supplied by the heat derived from the Boltzmann distribution of molecules.[43–47] Notably, FUCP-1 exhibited an excellent upconversion luminescence quantum yield (>12%) and outstanding photostability under 808 nm laser irradiation compared to Stokes excitation (700 nm). Moreover, FUCP-1 can effectively sensitize O_2 to $^1O_2$ and presented superior inhibition of 4T1 cells (the half maximal inhibitory concentration IC_{50} = 2.06 μM). After intravenous injection, FUCP-1 specially accumulated in the tumor sites and efficiently inhibited tumor growth

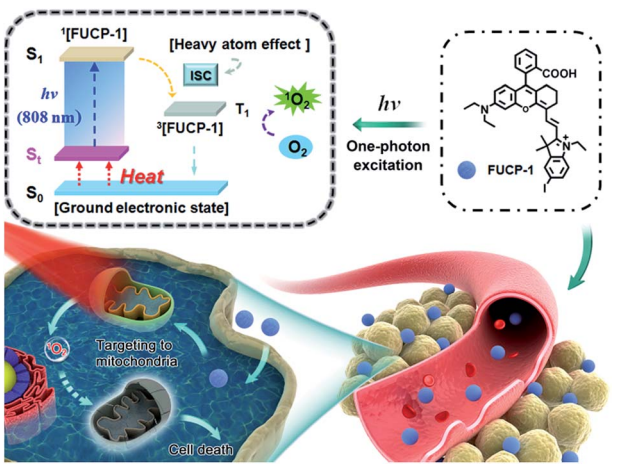

Fig. 1 Schematic illustration of the upconversion PDT process by a mitochondria-targeting photosensitizer (FUCP-1).

(~73.7%) after 808 nm laser irradiation. In addition, while the tumor was covered with 5 mm pork tissue and then exposed to the laser irradiation, the inhibition rate of tumor growth was still up to ~50.1%. Importantly, FUCP-1 could be easily cleared from the body within 24 h, demonstrating negligible systematic toxicity during treatment. All these advantages showed that this one-photon excitation molecular upconversion sensitizer FUCP-1 could serve as an ideal phototherapeutic platform for deep-seated cancer therapy.

Results and discussion

Synthesis and spectroscopy

FUCP-1 was efficiently prepared as outlined in Scheme S1.† Briefly, 5-iodo-2,3,3-trimethyl-3*H*-indole (1) was quaternized by iodoethane and then reacted with *N*,*N*′-diphenylformamidine to yield compound 2 (51.7% yield) which was further reacted with 3 to produce the final compound FUCP-1 (63.8% yield). The corresponding chemical structures were well characterized by ^{1}H NMR, ^{13}C NMR and ESI-MS (Fig. S1–S6†). To explore the upconversion emission properties of FUCP-1, spectral analysis was then conducted. Normalized UV-vis spectra in Fig. S7† showed that FUCP-1 possessed a strong absorption profile in the far-red visible region with a maximum at 715 nm ($\varepsilon = 1.3 \times 10^5$ L (mol^{-1} cm^{-1})) and presented considerably high NIR fluorescence centered at 750 nm. Meanwhile, under 808 nm excitation, FUCP-1 showed an intense NIR upconversion luminescence (UCL) signal, peaking at 750 nm, which was consistent with the emission upon Stokes excitation (700 nm). The UCL quantum yield (Φ_f) of FUCP-1 was up to 12.6% in dichloromethane which is superior to that of most nano-materials, favouring the application for image-guided cancer PDT.[48–50]

Upconversion luminescence mechanism of FUCP-1

To determine the mechanism for upconversion emission from FUCP-1, the effect of temperature on absorbance and fluorescent intensity (Stokes and anti-Stokes) was first studied. As shown in Fig. 2a and b, the intensity of absorbance obviously decreased as the solution temperature increased from 0 to 70 °C. Accordingly, the maximum fluorescence intensity of FUCP-1 rapidly decreased with increasing temperature.

It is noteworthy that the UCL intensity of FUCP-1 was significantly boosted as the solution temperature increased (Fig. 2c), consistent well with previous reports that higher temperature can facilitate the FUCL process.[37,46] In addition, the UCL intensity of FUCP-1 under 808 nm excitation showed superior linear dependence on the excitation power density from 0 to 52 mW cm^{-2} ($R^2 = 0.993$, Fig. 2d), suggesting that the UCL emission of FUCP-1 is an one-photon process. In view of the above two characteristics, we thus deduced that the one-photon upconversion luminescence process of FUCP-1 was indeed FUCL.[43,46,51,52] The upconversion luminescence mechanism of FUCP-1 is shown in Fig. 2e. Under low temperature conditions, a large percentage of FUCP-1 is in the zero point vibrational level of the ground electronic state (S_0). While the temperature increases, some of the molecules tend to distribute

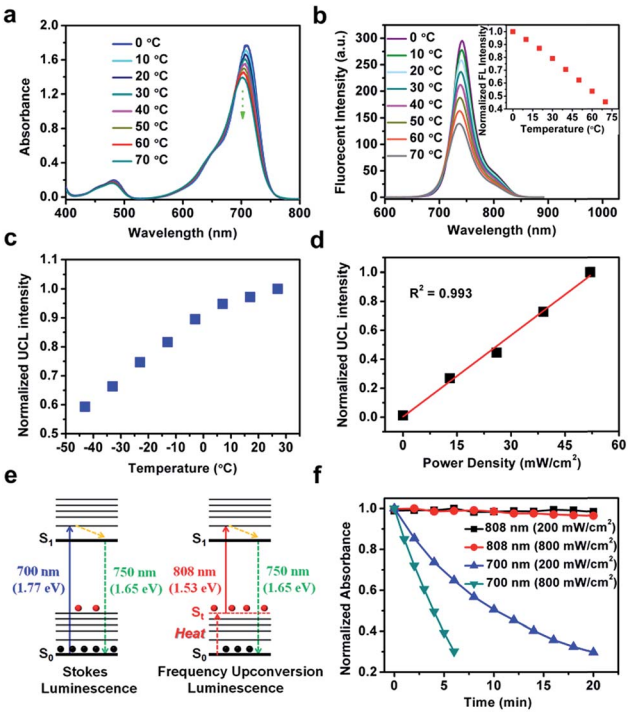

Fig. 2 (a) Absorption and (b) fluorescence intensity changes of FUCP-1 from 0 to 70 °C in ethanol. The inset shows normalized fluorescence changes at 742 nm at different temperatures. (c) UCL intensity changes of FUCP-1 (in ethanol) at different temperatures. (d) A plot of normalized UCL changes (λ_{ex} = 808 nm). (e) Schematic illustration of the mechanisms of Stokes luminescence and FUCL. (f) The photostability of FUCP-1 under 700 or 808 nm laser irradiation.

in the thermally vibrational–rotational states (S_t), leading to the absorption coefficient and Stokes emission from S_0 into S_1 to rapidly decline. In contrast, higher temperature facilitates the distribution of FUCP-1 to S_t, thereby resulting in excitation transition probabilities for anti-Stokes emission. We also calculated the photon energy of Stokes and anti-Stokes excitation. Obviously, the photon energy of 808 nm (1.53 eV) excitation is much lower than that of 700 nm (1.77 eV) excitation, which could dramatically enhance the anti-bleaching capabilities of dye molecules and reduce photodamage to normal tissue under anti-Stokes excitation.

Then, we conducted a photostability experiment (Fig. 2f). After exposure to continuous 808 nm laser illumination for 20 min (200 mW cm^{-2} or 800 mW cm^{-2}), nearly no photobleaching of the FUCP-1 solution was observed. In sharp contrast, under the same conditions as for traditional Stokes illumination (700 nm, 800 mW cm^{-2}), FUCP-1 was dramatically decomposed as indicated by the 70% decline of the absorption intensity in only 6 min (71% for 200 mW cm^{-2} in 20 min). The result indicates that FUCP-1 during the upconversion process displayed excellent anti-bleaching capabilities, which is critical for long-term imaging observation and photon-triggered cancer treatment.

$^{1}O_2$ photosensitizing ability of FUCP-1

In order to confirm the heavy atom effect of iodine atoms on the one-photon upconversion process, we then evaluated light-

triggered $^1O_2$ generation by using a specific commercial dye 1,3-diphenylisobenzofuran (DPBF, a molecular $^1O_2$ responder, Fig. S8†) and the corresponding non-halogenated FUCL analogue (NRh-1) as a comparison (Fig. 3a and b). After exposure to 808 nm laser (800 mW cm^{-2}) irradiation, the DPBF absorbance intensity sharply decreased within 240 s in the presence of FUCP-1 (Fig. S9†). In sharp contrast, when exposed to the same light dose (800 mW cm^{-2}, 240 s), negligible $^1O_2$ was generated by NRh-1 because of the lack of ISC capacity. DPBF decomposition at 415 nm by FUCP-1 with a 808 nm laser was 3.3-fold that of NRh-1, demonstrating that the introduction of the iodine atom immensely promoted the ISC process (Fig. 3c). We then investigated whether the temperature could affect the $^1O_2$ generation under upconversion excitation. When the solution temperature was boosted from −20 to 25 °C, the degradation rates of DPBF in FUCP-1 solution under 808 nm laser irradiation rapidly increased (Fig. 3d and S10†), showing that the promotion of excitation transition probabilities from upper vibrational–rotational states S_0 to S_1 as the temperature increases could effectively promote the distribution of FUCP-1 inT_1. These results clearly demonstrated that O_2 can be effectively sensitized to $^1O_2$ by the heavy atom effect during the one-photon upconversion process.

Next, to reveal the intracellular $^1O_2$ levels generated by FUCP-1, Singlet Oxygen Sensor Green (SOSG) was used as the $^1O_2$ capture agent.[53,54] As shown in Fig. S11,† no obvious fluorescence was observed in the groups NRh-1 with and without laser.

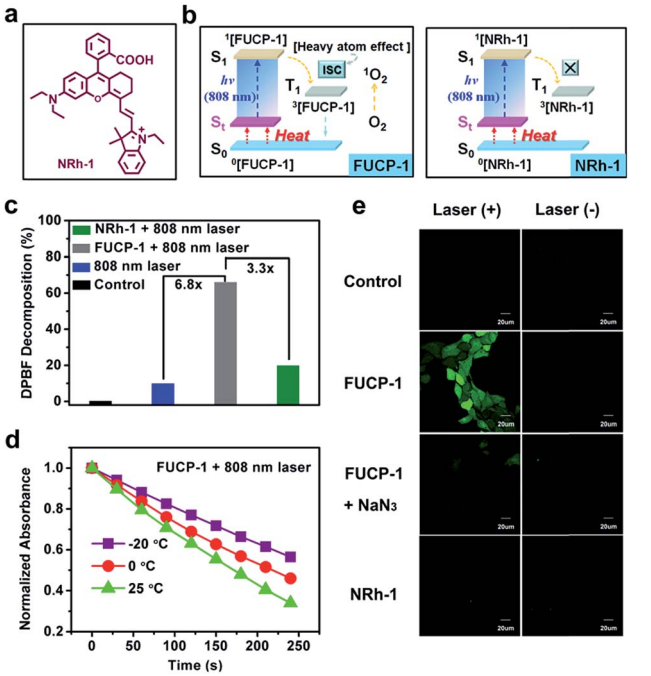

Fig. 3 (a) Chemical structure of NRh-1 (non-halogenated analogue). (b) Schematic illustration of $^1O_2$ photosensitizing by the heavy atom effect during the one-photon driven upconversion process. (c) DPBF decomposition at 415 nm for different groups. (d) The normalized absorbance changes of DPBF in the presence of FUCP-1 at different temperatures. (e) Confocal fluorescence images of 4T1 cells incubated with DCFH-DA (10 μM) under different treatments.

In contrast, strong green fluorescence was detected in 4T-1 cells treated with FUCP-1 and 808 nm laser irradiation, suggesting that O_2 can be effectively converted to $^1O_2$ in cancer cells by FUCP-1 under anti-Stokes excitation. We then further confirmed the species of ROS using 2′,7′-dichlorofluorescin diacetate (DCFH-DA) which is a well-used ROS capture agent. After incubation with DCFH-DA (10 μM) for 30 min, 4T1 cells which were treated with FUCP-1 (5 μM) and 808 nm laser irradiation (800 mW cm^{-2}, 10 min) showed intense green fluorescence of DCF (Fig. 3e). In contrast, 4T1 cells treated with NRh-1 with or without 808 nm laser irradiation did not show distinct fluorescence, which is in accordance with the result in Fig. S11.† Notably, the fluorescence induced by ROS in 4T1 cells was visibly quenched by NaN_3 (a widely accepted $^1O_2$ scavenger), further indicating that the species of ROS generated in the upconversion process by FUCP-1 was indeed $^1O_2$.

Cellular uptake and localization of FUCP-1

Prior to studying the potential PDT ability of FUCP-1, cellular uptake and subcellular localization was investigated in 4T1 cells. As presented in Fig. 4a and S12,† clear upconversion luminescence was detected in 4T1 cells only after 10 min of incubation with FUCP-1 and the upconversion luminescence rapidly peaked in 2–4 h. This result confirmed that the organic molecular dye FUCP-1 could effectively penetrate into the tumor cells, which is an important factor for *in vitro* and *in vivo* PDT. In addition, it was worth noting that the fluorescence distribution of FUCP-1 overlapped well with that of MitoTracker Green (a commercial mitochondrial tracking dye) with a high Pearson's correlation coefficient (PC = 0.87) (Fig. 4b). In contrast, very poor overlapping was observed in the group of Hoechst 33342 (a

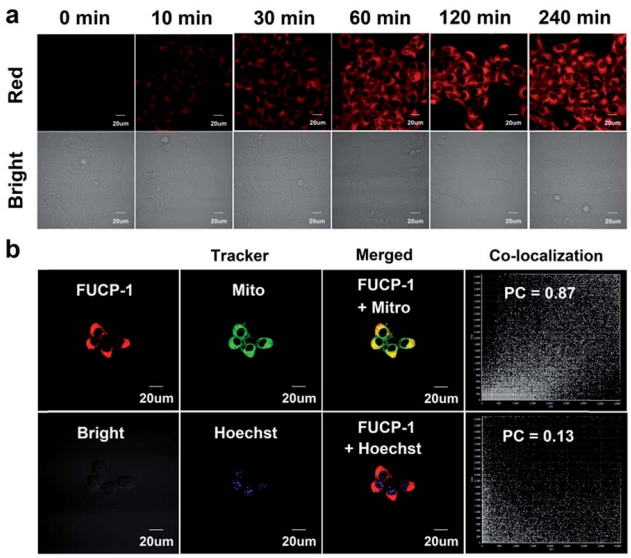

Fig. 4 (a) Confocal microscopy images of 4T-1 cells incubated with FUCP-1 (5 μM) for 0–240 min, excited at 808 nm. (b) Confocal microscopy images of FUCP-1 (5 μM) with various commercial trackers, MitoTracker Green (Mito) and Hoechst 33342 (Hoechst) in 4T1 cells, MitoTracker Green is 1 μM and Hoechst 33342 is 0.5 μM, PC is Pearson's correlation coefficient.

specific nuclear tracking dye) and FUCP-1 (PC = 0.13). These results demonstrated that FUCP-1 can well localize in mitochondria, presumably as the positive charge of the molecule directing the dye to the mitochondrion. This would result in efficient PDT, as the mitochondrion is of great importance for regulating various metabolic pathways in living cells.

In vitro one-photon upconversion excitation induced cellular toxicity evaluation

To investigate the potential PDT application of FUCP-1 during upconversion excitation, methyl thiazolyltetrazolium (MTT) assay was conducted based on 4T1 cancer cells. As shown in Fig. 5a, FUCP-1 with 808 nm laser irradiation presented superior inhibition of 4T1 cells and the half maximal inhibitory concentration (IC_{50}) was as low as 2.06 μM. In contrast, the groups only treated with FUCP-1 in the dark did not exhibit any obvious cell death, demonstrating its good biocompatibility. Moreover, with the optical density increased from 0 to 1.6 W cm^{-2}, FUCP-1 displayed significantly boosted cytotoxicity (Fig. 5b). Importantly, even under a high optical dose (1.6 W cm^{-2}, 10 min), the cell viabilities in the absence of FUCP-1 remained over 95%. The low photodamage was mainly due to the negligible absorption of water at this wavelength, well overcoming the defect of 980 nm excitation (water at this wavelength shows obvious absorption) widely used in traditional UCNPs.[55,56]

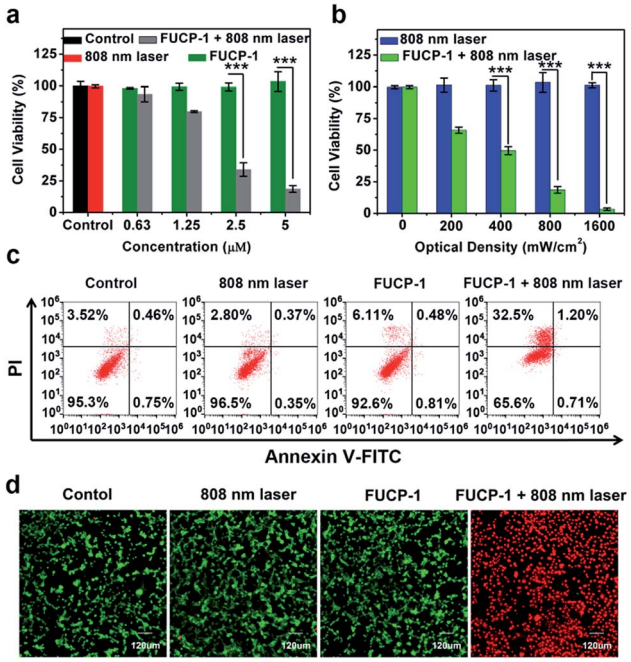

Fig. 5 (a) The viability of 4T1 cells incubated with 0–5 μM FUCP-1 in the dark or under 808 nm laser irradiation (800 mW cm^{-2}). (b) The viability of 4T1 cells incubated with FUCP-1 (5 μM) in the dark or under 808 nm laser irradiation at different optical densities (n = 3, data are expressed as mean ± SD, ***p < 0.001 determined by Student's t test). (c) Fluorescein annexin-V-FITC/PI double labeling flow cytometry results for 4T1 cells in different experimental groups. (d) Multichannel confocal fluorescence images in the green channel (λ_{ex} = 488 nm, λ_{em} = 505–555 nm) for calcein-AM stained live cells. Red channel (λ_{ex} = 559 nm, λ_{em} = 695–745 nm) for stained dead cells.

In order to understand the therapeutic mechanism, a flow cytometer was used to investigate the process of cell death. As depicted in Fig. 5c, 4T1 cell growth was not affected by treatments with PBS, FUCP-1 or 808 nm laser irradiation only. However, while 4T1 cells incubated with FUCP-1 were exposed to 808 nm laser irradiation, the percentage of necrotic cells rapidly increased to 32.5%, further demonstrating its promising application in PDT. A live/dead cell co-staining assay, in which the live and dead cells are labelled with green and red fluorescence respectively, was then conducted (Fig. 5d, S13†). Obviously, 4T1 cells treated with PBS, FUCP-1 or 808 nm laser irradiation showed intense green fluorescence. In contrast, 4T1 cells incubated with FUCP-1 (5 μM) followed by exposure to an 808 nm laser exhibited strong red fluorescence, intuitively showing the superior PDT ability of FUCP-1.

In vivo antitumor effect for deep-seated tumors

Encouraged by the excellent *in vitro* PDT performance of FUCP-1, we proceeded to study the anticancer efficacy *in vivo*. As tumor targeting was a very important characteristic for image-guided *in vivo* PDT,[57] we first evaluated the intratumoral accumulation of FUCP-1 in 4T1 tumor-bearing BALB/c mice *via* intravenous injection. As shown in Fig. 6a, FUCP-1 displayed outstanding tumor targeting and UCL imaging ability. Obviously, at 4 h and 8 h post-injection, the liver region exhibited an intense luminescence signal and then the UCL signal mainly shifted to the tumor site. The *ex vivo* UCL images at 8 h also demonstrated that FUCP-1 could accumulate in the tumor region efficiently (Fig. S14†). It was noticeable that the luminescence signal almost disappeared in mice 24 h post-injection, which demonstrated that FUCP-1 can be effectively cleared from the body, thus maximally reducing the long-term toxicity.

To demonstrate the *in vivo* PDT potential of FUCP-1 for deep-seated tumor imaging, 4T1 tumor-bearing BALB/c mice at 8 h after intravenous injection (1.2 mg kg^{-1} of FUCP-1), which was the maximum drug concentration time point at the tumor site, were exposed to 15 min irradiation (Fig. 6b). 5 mm pork tissue was prepared and used to cover the tumors in one of the treatment groups. During two weeks of therapy, the changes of tumor volumes and mice weights under different treatments (only PBS; FUCP-1 injection; only laser irradiation; FUCP-1 injection + 5 mm pork tissue + laser irradiation; FUCP-1 injection + laser irradiation) were simultaneously recorded. As presented in Fig. 6c, tumor volumes grew rapidly in these mice treated with PBS, FUCP-1 or only 808 nm laser irradiation (800 mW cm^{-2}, 15 min), suggesting that the tumor growth was not affected by FUCP-1 or 808 nm laser irradiation. By contrast, the irradiated mice at 8 h post-injection exhibited outstanding tumor inhibition. The inhibition rate of tumor growth was as high as ~73.7%, showing the prominent antitumor effect of FUCP-1. Importantly, the tumor was also significantly inhibited by FUCP-1 with 808 nm laser irradiation while 5 mm pork tissue covered the tumors during PDT (the inhibition rate of tumor growth was up to ~50.1%),

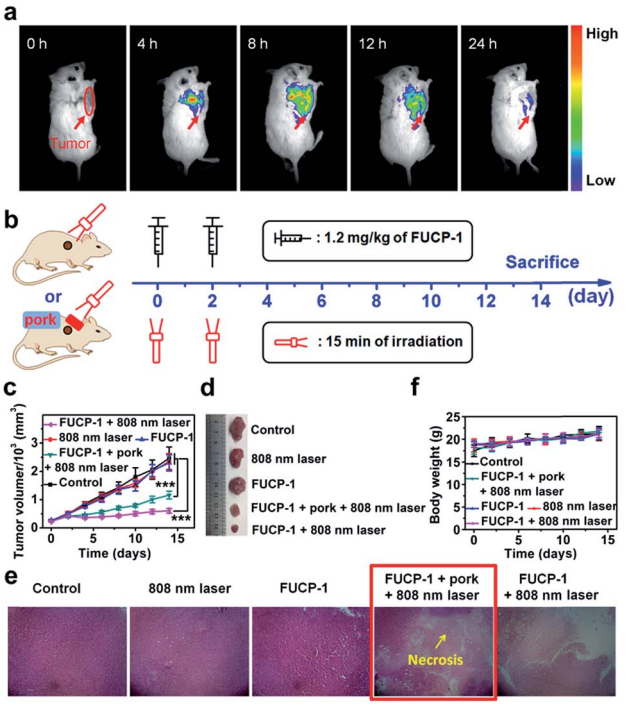

Fig. 6 (a) *In vivo* UCL imaging of FUCP-1 in 4T1 tumor-bearing BALB/c mice. (b) Experimental procedures. (c) Changes of tumor volumes obtained from the 4T1 tumor-bearing BALB/c mice under different treatments. Data are expressed as mean ± standard deviation ($n = 6$, data are expressed as mean ± SD, $^{***}p < 0.001$ determined by Student's *t* test). (d) Photographs of the corresponding tumors. (e) Hematoxylin & eosin (H&E) stained images of the dissected tumor tissues. (f) Body weight changes of the BALB/c mice under different treatments.

demonstrating the potential of FUCP-1 for deep-seated tumor treatment. These results were also represented using the representative photographs and average tumor weight of isolated tumors from the experimental mice after different treatments (Fig. 6d and S15†).

Hematoxylin and eosin (H&E) staining of the corresponding histological analysis showed that the treatment of FUCP-1 with 808 nm laser irradiation led to severe cell necrosis. Obviously, tumor tissue was also seriously injured while 5 mm pork tissue covered the tumors in the course of PDT (Fig. 6e). In contrast, no remarkable tumor tissue damage was observed when the mice were treated with only FUCP-1 or 808 nm laser irradiation. These results maintained good consistency with the data of tumor growth, further indicating that the one-photon driven PDT process of FUCP-1 could effectively result in tumor tissue ablation. In addition, all mice did not show apparent weight variation during the two weeks of therapy, suggesting that there were no negligible side effects caused by FUCP-1 and light irradiation (Fig. 6f). Histological analysis of the major organs was also performed. No noticeable damage was found from the H&E staining images of the heart, liver, spleen, lung, and kidney (Fig. S16†), confirming that FUCP-1 eliminated substantial systemic toxicity *in vivo* PDT treatment.

Conclusions

In summary, based on the FUCL strategy, we reported the first one-photon molecular upconversion photosensitizer (FUCP-1) with NIR 808 nm excitation and 750 nm emission for deep PDT. This new upconversion photosensitizer FUCP-1 showed a high UCL quantum yield which could help realize real-time monitoring of *in vivo* tumor-targeting accumulation. FUCP-1 demonstrated excellent photostability upon 808 nm laser irradiation, overcoming the photobleaching problem of traditional Stokes excitation. In addition, compared to traditional UCNPs which often suffer from unclear systematic toxicities, FUCP-1 could be easily cleared from the body within 24 h. More importantly, the *in vivo* PDT of FUCP-1 induced by a 808 nm laser displayed efficient antitumor efficacy while the tumors were covered with 5 mm pork tissue. Therefore, FUCP-1 is promising for photon-driven deep-seated cancer therapy and thus can be utilized as an ideal molecular upconversion platform for the design of multifunctional photosensitizers.

Conflicts of interest

The authors declare no competing financial interests.

Acknowledgements

This work was supported by the National Science Foundation of China (project 21421005, 21576037) and the NSFC-Liaoning United Fund U1608222. This study was conducted in accordance with the Guide for the Care and Use of Laboratory Animals published by the US National Institutes of Health (8th edition, 2011). The animal protocol was approved by the local research ethics review board of the Animal Ethics Committee of Dalian University of Technology (Certificate number//Ethics approval no. is 2018-043).

Notes and references

1 G. Yang, J. Tian, C. Chen, D. Jiang, Y. Xue, C. Wang, Y. Gao and W. Zhang, *Chem. Sci.*, 2019, **10**, 5766–5772.
2 M. Li, S. Long, Y. Kang, L. Guo, J. Wang, J. Fan, J. Du and X. Peng, *J. Am. Chem. Soc.*, 2018, **140**, 15820–15826.
3 M. Li, T. Xiong, J. Du, R. Tian, M. Xiao, L. Guo, S. Long, J. Fan, W. Sun, K. Shao, X. Song, J. W. Foley and X. Peng, *J. Am. Chem. Soc.*, 2019, **141**, 2695–2702.
4 Z. Yu, Y. Ge, Q. Sun, W. Pan, X. Wan, N. Li and B. Tang, *Chem. Sci.*, 2018, **9**, 3563–3569.
5 M. Li, J. Xia, R. Tian, J. Wang, J. Fan, J. Du, S. Long, X. Song, J. W. Foley and X. Peng, *J. Am. Chem. Soc.*, 2018, **140**, 14851–14859.
6 L. Yuan, W. Lin, Y. Yang and H. Chen, *J. Am. Chem. Soc.*, 2012, **134**, 1200–1211.
7 W. Fan, P. Huang and X. Chen, *Chem. Soc. Rev.*, 2016, **45**, 6488–6519.
8 N. M. Idris, M. K. Gnanasammandhan, J. Zhang, P. C. Ho, R. Mahendran and Y. Zhang, *Nat. Med.*, 2012, **18**, 1580.

9 S. Dong, J. Xu, T. Jia, M. Xu, C. Zhong, G. Yang, J. Li, D. Yang, F. He, S. Gai, P. Yang and J. Lin, *Chem. Sci.*, 2019, **10**, 4259–4271.
10 R. Bonnett, *Chem. Soc. Rev.*, 1995, **24**, 19–33.
11 M. R. Detty, S. L. Gibson and S. J. Wagner, *J. Med. Chem.*, 2004, **47**, 3897–3915.
12 X. Miao, W. Hu, T. He, H. Tao, Q. Wang, R. Chen, L. Jin, H. Zhao, X. Lu, Q. Fan and W. Huang, *Chem. Sci.*, 2019, **10**, 3096–3102.
13 R. Hota, K. Baek, G. Yun, Y. Kim, H. Jung, K. M. Park, E. Yoon, T. Joo, J. Kang, C. G. Park, S. M. Bae, W. S. Ahn and K. Kim, *Chem. Sci.*, 2013, **4**, 339–344.
14 S. Luo, X. Tan, Q. Qi, Q. Guo, X. Ran, L. Zhang, E. Zhang, Y. Liang, L. Weng, H. Zheng, T. Cheng, Y. Su and C. Shi, *Biomaterials*, 2013, **34**, 2244–2251.
15 T.-C. Chen, L. Huang, C.-C. Liu, P.-J. Chao and F.-H. Lin, *Process Biochem.*, 2012, **47**, 1903–1908.
16 F. Li, Y. Du, J. Liu, H. Sun, J. Wang, R. Li, D. Kim, T. Hyeon and D. Ling, *Adv. Mater.*, 2018, **30**, 1870264.
17 J. B. Jarman and D. A. Dougherty, *Chem. Commun.*, 2019, **55**, 5511–5514.
18 J. Atchison, S. Kamila, H. Nesbitt, K. A. Logan, D. M. Nicholas, C. Fowley, J. Davis, B. Callan, A. P. McHale and J. F. Callan, *Chem. Commun.*, 2017, **53**, 2009–2012.
19 X. Zhu, Q. Su, W. Feng and F. Li, *Chem. Soc. Rev.*, 2017, **46**, 1025–1039.
20 J. Xu, W. Han, P. Yang, T. Jia, S. Dong, H. Bi, A. Gulzar, D. Yang, S. Gai, F. He, J. Lin and C. Li, *Adv. Funct. Mater.*, 2018, **28**, 1803804.
21 Z. Yang, K. Y. Loh, Y.-T. Chu, R. Feng, N. S. R. Satyavolu, M. Xiong, S. M. Nakamata Huynh, K. Hwang, L. Li, H. Xing, X. Zhang, Y. R. Chemla, M. Gruebele and Y. Lu, *J. Am. Chem. Soc.*, 2018, **140**, 17656–17665.
22 T. Liang, Z. Li, P. Wang, F. Zhao, J. Liu and Z. Liu, *J. Am. Chem. Soc.*, 2018, **140**, 14696–14703.
23 L. Huang, Y. Zhao, H. Zhang, K. Huang, J. Yang and G. Han, *Angew. Chem., Int. Ed.*, 2017, **56**, 14400–14404.
24 W. W. Zheng, P. Huang, D. Tu, E. Ma, H. Zhu and X. Chen, *Chem. Soc. Rev.*, 2015, **44**, 1379–1415.
25 A. Gnach, T. Lipinski, A. Bednarkiewicz, J. Rybka and J. A. Capobianco, *Chem. Soc. Rev.*, 2015, **44**, 1561–1584.
26 Y. Sun, W. Feng, P. Yang, C. Huang and F. Li, *Chem. Soc. Rev.*, 2015, **44**, 1509–1525.
27 Y. Liu, Q. Su, X. Zou, M. Chen, W. Feng, Y. Shi and F. Li, *Chem. Commun.*, 2016, **52**, 7466–7469.
28 A. B. Chinen, C. M. Guan, J. R. Ferrer, S. N. Barnaby, T. J. Merkel and C. A. Mirkin, *Chem. Rev.*, 2015, **115**, 10530–10574.
29 S. Gai, C. Li, P. Yang and J. Lin, *Chem. Rev.*, 2014, **114**, 2343–2389.
30 L. Cheng, C. Wang and Z. Liu, *Nanoscale*, 2013, **5**, 23–37.
31 S. Han, R. Deng, X. Xie and X. Liu, *Angew. Chem., Int. Ed.*, 2014, **53**, 11702–11715.
32 H. S. Jung, J.-H. Lee, K. Kim, S. Koo, P. Verwilst, J. L. Sessler, C. Kang and J. S. Kim, *J. Am. Chem. Soc.*, 2017, **139**, 9972–9978.
33 F. Peng, M. Setyawati, J. Kai Tee, X. Ding, J. Wang, M. En Nga, H. Ho and D. Leong, *Nat. Nanotechnol.*, 2019, **14**, 279–286.
34 D. A. Ammar, T. C. Lei, O. Masihzadeh, E. A. Gibson and M. Y. Kahook, *Mol. Vision*, 2011, **17**, 583–590.
35 H. Yang, C. Han, X. Zhu, Y. Liu, K. Y. Zhang, S. Liu, Q. Zhao, F. Li and W. Huang, *Adv. Funct. Mater.*, 2016, **26**, 1945–1953.
36 Y. Liu, Q. Su, M. Chen, Y. Dong, Y. Shi, W. Feng, Z.-Y. Wu and F. Li, *Adv. Mater.*, 2016, **28**, 6625–6630.
37 Y. Li, Y. Deng, J. Liu, J. Fu, Y. Sun, R. Ouyang and Y. Miao, *Sens. Actuators, B*, 2019, **286**, 337–345.
38 J. Jiang, Y. Qian, Z. Xu, Z. Lv, P. Tao, M. Xie, S. Liu, W. Huang and Q. Zhao, *Chem. Sci.*, 2019, **10**, 5085–5094.
39 T. Yogo, Y. Urano, Y. Ishitsuka, F. Maniwa and T. Nagano, *J. Am. Chem. Soc.*, 2005, **127**, 12162–12163.
40 Y. Cai, P. Liang, Q. Tang, X. Yang, W. Si, W. Huang, Q. Zhang and X. Dong, *ACS Nano*, 2017, **11**, 1054–1063.
41 I. S. Turan, D. Yildiz, A. Turksoy, G. Gunaydin and E. U. Akkaya, *Angew. Chem., Int. Ed.*, 2016, **55**, 2875–2878.
42 Q. Guan, L.-L. Zhou, Y.-A. Li and Y.-B. Dong, *Inorg. Chem.*, 2018, **57**, 10137–10145.
43 D. Bloor, G. Cross, P. K. Sharma, J. A. Elliott and G. Rumbles, *J. Chem. Soc., Faraday Trans.*, 1993, **89**, 4013–4015.
44 B. Stevens, *Chem. Rev.*, 1957, **57**, 439–477.
45 A. N. Kuzmin, A. Baev, A. V. Kachynski, T. S. Fisher, A. Shakouri and P. N. Prasad, *J. Appl. Phys.*, 2011, **110**, 033512.
46 Z. Dong, Q. Han, Z. Mou, G. Li and W. Liu, *J. Mater. Chem. B*, 2018, **6**, 1322–1327.
47 J. L. Clark, P. F. Miller and G. Rumbles, *J. Phys. Chem. A*, 1998, **102**, 4428–4437.
48 C. Homann, L. Krukewitt, F. Frenzel, B. Grauel, C. Würth, U. Resch-Genger and M. Haase, *Angew. Chem., Int. Ed.*, 2018, **57**, 8765–8769.
49 S. Fischer, N. D. Bronstein, J. K. Swabeck, E. M. Chan and A. P. Alivisatos, *Nano Lett.*, 2016, **16**, 7241–7247.
50 N. J. J. Johnson, S. He, S. Diao, E. M. Chan, H. Dai and A. Almutairi, *J. Am. Chem. Soc.*, 2017, **139**, 3275–3282.
51 J. L. Clark and G. Rumbles, *Phys. Rev. Lett.*, 1996, **76**, 2037–2040.
52 M. H. Bartl, B. J. Scott, G. Wirnsberger, A. Popitsch and G. D. Stucky, *ChemPhysChem*, 2003, **4**, 392–395.
53 A. P. Thomas, L. Palanikumar, M. T. Jeena, K. Kim and J.-H. Ryu, *Chem. Sci.*, 2017, **8**, 8351–8356.
54 J. Tian, J. Zhou, Z. Shen, L. Ding, J.-S. Yu and H. Ju, *Chem. Sci.*, 2015, **6**, 5969–5977.
55 S. He, N. J. J. Johnson, V. A. Nguyen Huu, Y. Huang and A. Almutairi, *Chem. Mater.*, 2018, **30**, 3991–4000.
56 F. Ai, Q. Ju, X. Zhang, X. Chen, F. Wang and G. Zhu, *Sci. Rep.*, 2015, **5**, 10785.
57 M.-K. Zhang, X.-G. Wang, J.-Y. Zhu, M.-D. Liu, C.-X. Li, J. Feng and X.-Z. Zhang, *Small*, 2018, **14**, 1800292.